Fifth International Conference on Advanced COmputational Methods in ENgineering (ACOMEN 2011)
Liège, Belgium, 14-17 November 2011

Full discontinuous Galerkin formulation of shell in large deformations with fracture mechanic applications

G. Becker[1]*and L. Noels[1]

[1] Aerospace and Mechanical Engineering Department (LTAS-cm3),
University of Liège, Chemin des chevreuils 1, 4000 Liège, Belgium

e-mails: *gauthier.becker@ulg.ac.be*, *l.noels@ulg.ac.be*

Abstract

Different methods have been developed to model tearing prediction, as *e.g.*, the combination between the cohesive principle and the finite element method. Unfortunately, this method has some well known issues that can be fixed by recourse to discontinuous Galerkin formulation. Such a formulation allows to insert very easily an extrinsic cohesive element at onset of fracture without any mesh modification. This promising technique has been recently developed by the authors for linear shell. Although promising numerical results were obtained, it is difficult to compare the method with experiments due to the large plastic deformation present in material before the fracture apparition. Thus, the method is extent herein to elasto-plastic finite deformations. The simulations of some benchmarks prove the ability of this new framework to model accurately the continuum part of the deformation and the crack propagation.

1 Introduction

For economic and environmental reasons, the industrial use of raw material is streamlined. It leads to the thickness reduction of some components that can exhibit fracture and therefore increase the interest for tearing prediction modeling. Some numerical techniques were developed to take into account such a phenomenon and among of them, the cohesive approach was combined with finite element method. As cohesive element models the separation work between the crack lips it can suitably be inserted between two finite elements to model crack initiation or propagation between them. Unfortunately, this insertion presents some issues. Indeed, if this one is performed at the beginning of the simulation, the cohesive law is called intrinsic, and has to model the continuous part of the deformation. This cannot be realized in a consistent way and leads therefore to inaccurate results. On the contrary, the insertion during the simulation allows to use extrinsic cohesive law but requires mesh modifications. In fact, to insert the cohesive element the nodes have to be duplicated leading to a very complex implementation, especially in the case of a parallel one.

One method (among others) that can be used to solve these issues is the combination between discontinuous Galerkin formulation and an extrinsic cohesive law as it has been pioneered by Mergheim *et al.* [1] and by Radovitzky *et al.* [2]. The discontinuous Galerkin method allows to model (weakly) the continuum part of deformation in a consistent way with discontinuous elements. When a fracture appears, this discontinuity can be exploited to insert a cohesive element without mesh modification. The authors have recently extended this combination to thin structures (discretized with beam, plate or shell elements) under the assumption of linear elasticity [3, 4].

This assumption limits the applicability of the method, which seems nevertheless very promising, as very few materials present small elastic strains before the apparition of fracture. Thus, the authors extend

*PhD candidate at the Belgian National Fund for Education at the Research in Industry and Farming (FNRS)

their formulation to elasto-plastic finite deformations to model in a more accurate way the behavior of material before the crack initiation or propagation [5]. This extension is developed from [6] and [4].

The presented method is validated with some numerical benchmarks. On the one hand, the method is used to model continuum mechanic problems and it is proved by comparison with the literature that the method is able to simulate quasi-static or dynamic problems as accurately as other traditional shell formulations. On the other hand, the benchmark considering the blast of a pressurized cylinder presented by Larsson *et al.* [7] is simulated with the new model to show that the extension allows to obtain results close from experiment.

2 Continuum mechanic of thin bodies

The continuum mechanic of thin bodies is summarized in this section. Mechanic of thin bodies can be found in several references [4, 6, 8, 9, 10, 11, 12, 13] among others. In particular the two first cited, use exactly the same notations than this paper.

2.1 Notation

Hereinafter, a subscript will be used to refer to values expressed in the considered basis, while a superscript will be used to refer to values expressed in the conjugate basis. Roman letters as a subscript or superscript substitute for integers between one and three, while Greek letters substitute for integers one or two.

2.2 Kinematic of thin bodies

The kinematic of thin bodies, represented on figure 1, can be described by considering its mid-surface section as a Cosserat plane $\mathcal{A}$ and a third coordinate, representing the thickness, belonging to the interval $[h_{\min};\, h_{\max}]$. In the reference frame $\boldsymbol{E}_I$, this representation is written $\boldsymbol{\xi} = \sum_{I=1}^{3} \xi^I \boldsymbol{E}_I$: $\mathcal{A} \times [h_{\min};\, h_{\max}] \rightarrow \mathbb{R}^3$. Using $\boldsymbol{\varphi}\left(\xi^1,\, \xi^2\right) : \mathcal{A} \rightarrow \mathbb{R}^3$ the mapping of the mid-surface and $\boldsymbol{t}$: $\mathcal{A} \rightarrow \mathrm{S}^2 = \left\{\boldsymbol{t} \in \mathbb{R}^3 |_{\|\boldsymbol{t}\|=1}\right\}$ the director of the mid-surface, with S^2 the unit sphere manifold, a configuration $\mathcal{S}$ of the shell is represented by the manifold of position $\boldsymbol{x}$, which is obtained by the mapping $\boldsymbol{\Phi} : \mathcal{A} \times [h_{\min};\, h_{\max}] \rightarrow \mathcal{S}$,

$$\boldsymbol{x} \;=\; \boldsymbol{\Phi}\left(\xi^I\right) = \boldsymbol{\varphi}\left(\xi^\alpha\right) + \xi^3 \lambda_h \boldsymbol{t}\left(\xi^\alpha\right) . \tag{1}$$

where λ_h is the thickness stretch of the shell. By convention, $\mathcal{S}$ refers to the current configuration of the shell, while the reference configuration $\mathcal{S}_0$ is obtained by the mapping $\boldsymbol{\Phi}_0$.

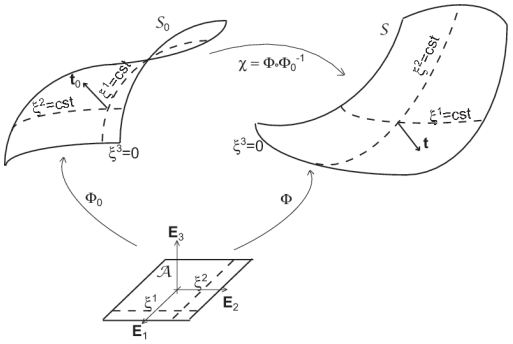

Figure 1: Description of the different configurations of the shell.

Finally, the two points deformation gradient between these two configurations can be written

$$\mathbf{F} \;=\; \boldsymbol{\varphi}_{,\alpha} \otimes \boldsymbol{g}_0^\alpha + \xi^3 \lambda_h \boldsymbol{t}_{,\alpha} \otimes \boldsymbol{g}_0^\alpha + \lambda_h \boldsymbol{t} \otimes \boldsymbol{g}_0^3 \,, \tag{2}$$

where,

$$\boldsymbol{g}_\alpha = \frac{\partial \boldsymbol{\Phi}}{\partial \xi^\alpha} = \boldsymbol{\varphi}_{,\alpha} + \xi^3 \lambda_h \boldsymbol{t}_{,\alpha} + \xi^3 \boldsymbol{t} \lambda_{h,\alpha} \text{ and } \boldsymbol{g}_3 = \frac{\partial \boldsymbol{\Phi}}{\partial \xi^3} = \lambda_h \boldsymbol{t}\,, \tag{3}$$

2.3 Governing equations of shell

The governing equations of a thin body are obtained by integrating on the thickness the equations of force and moment equilibrium, leading to

$$\overline{\rho}\ddot{\boldsymbol{\varphi}} - \frac{1}{\bar{j}} \left(\bar{j}\boldsymbol{n}^\alpha\right)_{,\alpha} = 0 \quad \text{on } \mathcal{A}, \text{ and} \tag{4}$$

$$\frac{1}{\bar{j}} \left(\bar{j}\tilde{\boldsymbol{m}}^\alpha\right)_{,\alpha} - \boldsymbol{l} + \lambda \boldsymbol{t} = 0 \quad \text{on } \mathcal{A}\,, \tag{5}$$

where λ is an undefined pressure, $\overline{\rho} = h\rho$ is the density by unit of surface with h the thickness and with the jacobian $\bar{j} = \|\boldsymbol{\varphi}_{,1} \wedge \boldsymbol{\varphi}_{,2}\|$. Furthermore, the integration on the thickness of the Cauchy stress tensor $\boldsymbol{\sigma}$ [8, 9] leads to the definition of

$$\boldsymbol{n}^\alpha = \frac{1}{\bar{j}} \int_{h_{\min 0}}^{h_{\max 0}} \boldsymbol{\tau}\boldsymbol{g}^\alpha \det\left(\boldsymbol{\nabla}\boldsymbol{\Phi}_0\right) d\xi^3\,, \tag{6}$$

$$\boldsymbol{m}^\alpha = \frac{\lambda_h}{\bar{j}} \boldsymbol{t} \wedge \int_{h_{\min 0}}^{h_{\max 0}} \xi^3 \boldsymbol{\tau}\boldsymbol{g}^\alpha \det\left(\boldsymbol{\nabla}\boldsymbol{\Phi}_0\right) d\xi^3 = \lambda_h \boldsymbol{t} \wedge \tilde{\boldsymbol{m}}^\alpha\,, \text{ and} \tag{7}$$

$$\boldsymbol{l} = \frac{1}{\bar{j}} \int_{h_{\min 0}}^{h_{\max 0}} \boldsymbol{\tau}\boldsymbol{g}^3 \det\left(\boldsymbol{\nabla}\boldsymbol{\Phi}_0\right) d\xi^3\,, \tag{8}$$

respectively the resultant stress vector, the resultant torque vector and the resultant across-the-thickness stress vector written in term of the Kirchhoff stress tensor $\boldsymbol{\tau} = J\boldsymbol{\sigma}$ for more convenience with the material law. Note that in equations (4) and (5) inertial angular forces are neglected[1] and the external forces are not considered.

In order to define the stress components, the resultant stress vectors are decomposed in the convected basis, as

$$\boldsymbol{n}^\alpha = n^{\alpha\beta}\boldsymbol{\varphi}_\beta + \lambda_h l^\alpha \boldsymbol{t} = \left(\tilde{n}^{\alpha\beta} + \lambda_\mu^\beta \tilde{m}^{\alpha\mu}\right)\boldsymbol{\varphi}_\beta + \lambda_h l^\alpha \boldsymbol{t}\,, \tag{9}$$

$$\boldsymbol{l} = l^\alpha \boldsymbol{\varphi}_\alpha\,, \text{ and} \tag{10}$$

$$\tilde{\boldsymbol{m}}^\alpha = \tilde{m}^{\alpha\beta}\boldsymbol{\varphi}_\beta + \lambda_h \tilde{m}^{3\alpha}\boldsymbol{t}\,. \tag{11}$$

In these expressions, $\tilde{n}^{\alpha\beta}$ is the membrane stress, $\tilde{m}^{\alpha\beta}$ is the stress couple resultant, l^α is the out-of-plane stress resultant, $\tilde{m}^{\alpha 3}$ is the out-of-plane stress couple and $\lambda_\mu^\beta = \lambda_h \boldsymbol{t}_\mu \cdot \boldsymbol{\varphi}^{,\beta}$ characterizes the curvature of the shell. Under Kirchhoff-Love shell assumption, l^α can be neglected, but it is kept temporarily in the equations in order to develop the full-DG formulation.

This set of governing equations is accompanied by conventional boundary conditions applied on the boundary $\partial\mathcal{A}$ of the mid-surface $\mathcal{A}$ (see [13] for details).

2.4 Constitutive behavior

The previous set of equations is completed by a constitutive relation linking the deformations to the stresses. The plastic behavior of material is taken into account thanks to the J_2-flow theory with an isotropic linear hardening. The model is based on hyperelastic formulation, which implies the assumption of a multiplicative decomposition of deformation gradient $\mathbf{F}$ into an elastic part $\mathbf{F}^e$ and a plastic

[1] The inertial angular forces can be neglected if the thickness is sufficiently thin which is usually the case for thin bodies formulations.

part $\mathbf{F}^p$. With the assumption of an elastic part of a material law, which is the derivative of a potential W, the bi-logarithmic potential reads,

$$W\left(\mathbf{C}^e\right) \quad = \quad \frac{K}{2}\log J^2 + \frac{G}{4}\log \mathbf{C}^e : \log \mathbf{C}^e \tag{12}$$

with K and G respectively the bulk and shear Moduli of material. As W should only depends on the elastic deformation, it is the elastic right Cauchy strain tensor which is considered in (12), defined by $\mathbf{C}^e = \left(\mathbf{F}^e\right)^T \mathbf{F}^e$. Using these definitions the first Piola-Kirchhoff stress tensor can be written,

$$\mathbf{P} \quad = \quad 2\mathbf{F}\cdot\left[\left(\mathbf{F}^p\right)^{-1}\frac{\partial W\left(\mathbf{C}^e\right)}{\partial \mathbf{C}^e}\left(\mathbf{F}^p\right)^{-T}\right] \tag{13}$$

Then, the incremental theory can be used to determine the stresses at stage $n+1$ from the known values at stage n as it is described in [14, 15].

Finally, the determination of thickness stretch (λ_h) has to be specified. The thickness is discretized with 11 integration points following a Simpson integration rule. Then, the local λ_h^p is determined at each point by Newton-Raphson iterations satisfying locally the plane stress requirement $\tau^{33} = 0$. To achieve this, the Kirchhoff stress tensor $\boldsymbol{\tau} = \mathbf{P}\mathbf{F}^T$ is expressed in the convected basis thanks to

$$\tau^{ij} = \tau_{ij}\boldsymbol{g}^i \otimes \boldsymbol{g}^j \tag{14}$$

The global thickness stretch λ_h is then determined by the Simpson integration on the 11 local values λ_h^p.

3 Discontinuous Galerkin formulation of shell

The equation system defined by (4-5) can be solved using a finite element method. This one considers a weak form of the system and a discretization of $\mathcal{A}$ in elements. Furthermore, instead of seeking the exact solution $\boldsymbol{\varphi}$, a polynomial approximation $\boldsymbol{\varphi}_h$ constitutes the solution of the finite element problem. In continuous Galerkin formulation, this approximation is continuous from one element to its neighbors ensuring in this way the continuity of the solution. Moreover, for thin bodies, the continuity of first derivative of $\boldsymbol{\varphi}$ has to be verify to guarantee to curvature of shell. However, the traditional Lagrangian interpolation does not satisfy this requirement but it can be guaranteed weakly within a discontinuous Galerkin framework. This weak enforcement allows to obtain a one field (displacement) formulation and has been previously developed by authors first in the linear case [13] and extended in a second time to non linear shell [6]. Recently, with the aim to take into account initiation and propagation of fracture, this formulation was extended to discontinuous polynomial approximation for linear beam [3] and shell [4]. This paper develops the same approach but is applied now to non linear shell finite deformation.

3.1 Weak form of the problem

The discontinuous Galerkin frameworks introduces 3 interfaces terms

1. **consistency term:** This one results directly of the discontinuous approximation of the solution considering the jump between two elements. This jump can be replaced by a consistent numerical flux which is here the traditional average flux.

2. **compatibility term:** This one is introduced to ensure (weakly) the continuity of solution across element boundaries.

3. **stability term:** This one is introduced to ensure stability as it is well known that for elliptic problems discontinuous Galerkin formulation leads to unstabilities. Exactly as the compatibility term, the introduction of this term does not modify the consistency of the method. The stability term depends on a stability parameter which is independent of mesh size and material properties.

These 3 terms can be developed to ensure continuity of derivative for non linear shell as presented in [6]

$$a^s_{mI1}(\boldsymbol{\varphi}_h, \delta\boldsymbol{\varphi}) = \int_s \langle \bar{j}\lambda_h \tilde{\boldsymbol{m}}^\alpha \rangle \cdot [\![\delta \boldsymbol{t}]\!]\, \nu^-_\alpha d\partial\mathcal{A}_e \tag{15}$$

$$a^s_{mI2}(\boldsymbol{\varphi}_h, \delta\boldsymbol{\varphi}) = \int_s [\![\boldsymbol{t}]\!] \cdot \left\langle \bar{j}_0 \mathcal{H}^{\alpha\beta\gamma\delta}_m \left(\delta\boldsymbol{\varphi}_{,\gamma}\cdot\boldsymbol{t}_{,\delta} + \boldsymbol{\varphi}_{,\gamma}\cdot\delta\boldsymbol{t}_{,\delta}\right)\boldsymbol{\varphi}_{,\beta} + \bar{j}\lambda_h\tilde{\boldsymbol{m}}^\alpha\cdot\boldsymbol{\varphi}_{,\beta}\delta\boldsymbol{\varphi}_{,\beta}\right\rangle \nu^-_\alpha d\partial\mathcal{A}_e \tag{16}$$

$$a^s_{mI3}(\boldsymbol{\varphi}_h, \delta\boldsymbol{\varphi}) = \int_s [\![\boldsymbol{t}\,(\boldsymbol{\varphi}_h)]\!]\cdot\boldsymbol{\varphi}_{,\beta}\left\langle \frac{\beta_1 \mathcal{H}^{\alpha\beta\gamma\delta}_m \bar{j}_0}{h^s}\right\rangle [\![\delta\boldsymbol{t}]\!]\cdot\boldsymbol{\varphi}_{,\gamma}\nu^-_\alpha\nu^-_\delta d\partial\mathcal{A}_e \tag{17}$$

$$\tag{18}$$

which are consistency (15) compatibility (16) and stability (17) terms. In the last equation, β_1 is the dimensionless stability parameter, h^s the characteristic size of the element. Finally, $\mathcal{H}_m$ is the linearized bending stiffness,

$$\mathcal{H}^{\alpha\beta\gamma\delta}_m = \frac{E\left(h_{max}-h_{min}\right)^3}{12\left(1-\nu^2\right)}\Big[\nu\boldsymbol{\varphi}_0^{,\alpha}\cdot\boldsymbol{\varphi}_0^{,\beta}\boldsymbol{\varphi}_0^{,\gamma}\cdot\boldsymbol{\varphi}_0^{,\delta} + \frac{1}{2}\left(1-\nu\right)\boldsymbol{\varphi}_0^{,\alpha}\cdot\boldsymbol{\varphi}_0^{,\gamma}\boldsymbol{\varphi}_0^{,\beta}\cdot\boldsymbol{\varphi}_0^{,\delta} + \frac{1}{2}(1-\nu)\boldsymbol{\varphi}_0^{,\alpha}\cdot\boldsymbol{\varphi}_0^{,\delta}\boldsymbol{\varphi}_0^{,\beta}\cdot\boldsymbol{\varphi}_0^{,\gamma}\Big] \tag{19}$$

with E and ν respectively the Young modulus and the Poisson ratio of the material.

The additional terms related to the full discontinuous Galerkin framework can be developed for the non linear case following exactly the same argumentation developed in [4] and [6] for equations (15-17) which gives,

$$a^s_{nI1}(\boldsymbol{\varphi}_h, \delta\boldsymbol{\varphi}) = \int_s \langle \bar{j}\boldsymbol{n}^\alpha\rangle\cdot[\![\delta\boldsymbol{\varphi}]\!]\,\nu^-_\alpha d\partial\mathcal{A}_e \tag{20}$$

$$a^s_{nI2}(\boldsymbol{\varphi}_h, \delta\boldsymbol{\varphi}) = \int_s [\![\boldsymbol{\varphi}_h]\!]\cdot\langle\delta\left(\bar{j}\boldsymbol{n}^\alpha\right)\rangle\,\nu^-_\alpha d\partial\mathcal{A}_e \tag{21}$$

$$a^s_{nI3}(\boldsymbol{\varphi}_h, \delta\boldsymbol{\varphi}) = \int_s [\![\boldsymbol{\varphi}_h]\!]\cdot\boldsymbol{\varphi}_{,\gamma}\nu^-_\delta\left\langle\frac{\beta_2\mathcal{H}^{\alpha\beta\gamma\delta}_n\bar{j}_0}{h^s}\right\rangle[\![\delta\boldsymbol{\varphi}]\!]\cdot\boldsymbol{\varphi}_\beta\nu^-_\alpha d\partial\mathcal{A}_e \tag{22}$$

$$a^s_{sI3}(\boldsymbol{\varphi}_h, \delta\boldsymbol{\varphi}) = \int_s [\![\boldsymbol{\varphi}_h]\!]\cdot\boldsymbol{t}\nu^-_\beta\left\langle\frac{\beta_3\mathcal{H}^{\alpha\beta}_q\bar{j}_0}{h^s}\right\rangle[\![\delta\boldsymbol{\varphi}]\!]\cdot\boldsymbol{t}\nu^-_\alpha d\partial\mathcal{A}_e \tag{23}$$

respectively the consistency membrane (20), the compatibility membrane (21), the stability membrane (22) and the stability shearing (23) terms. In these equations β_2 and β_3 are dimensionless stability parameters and $\mathcal{H}_n$ and $\mathcal{H}_q$ are respectively the linearized membrane and shearing stiffness given by,

$$\mathcal{H}^{\alpha\beta\gamma\delta}_n = \frac{E\left(h_{max}-h_{min}\right)}{1-\nu^2}\Big[\nu\boldsymbol{\varphi}_0^{,\alpha}\cdot\boldsymbol{\varphi}_0^{,\beta}\boldsymbol{\varphi}_0^{,\gamma}\cdot\boldsymbol{\varphi}_0^{,\delta} + \frac{1}{2}\left(1-\nu\right)\boldsymbol{\varphi}_0^{,\alpha}\cdot\boldsymbol{\varphi}_0^{,\gamma}\boldsymbol{\varphi}_0^{,\beta}\cdot\boldsymbol{\varphi}_0^{,\delta} + \frac{1}{2}(1-\nu)\boldsymbol{\varphi}_0^{,\alpha}\cdot\boldsymbol{\varphi}_0^{,\delta}\boldsymbol{\varphi}_0^{,\beta}\cdot\boldsymbol{\varphi}_0^{,\gamma}\Big] \tag{24}$$

$$\mathcal{H}^{\alpha\beta}_q = G\left(h_{max}-h_{min}\right)\boldsymbol{\varphi}_0^\alpha\cdot\boldsymbol{\varphi}_0^\beta \tag{25}$$

The 3 first terms ensure a consistent and stable continuity in the Cosserat plane of the mid-surface of the shell. The last one guarantee the continuity of the out-of-plane displacement. As lengthy described in [3, 4] this one is obtained by considering the shearing components in the development of the equations. As Kirchhoff-Love assumption neglects shearing the consistency and compatibility terms can be neglected in such a way that only the stability term remains. The linearized expression of $\delta\left(\bar{j}\boldsymbol{n}^\alpha\right)$ necessitates

some development but is similarly as the linearization of $\delta\left(\bar{j}\tilde{\boldsymbol{m}}^{\alpha}\right)$ performed in [6],

$$\begin{aligned}
\delta\left(\bar{j}\boldsymbol{n}^{\alpha}\right) &= \frac{\bar{j}_0}{2}\mathcal{H}_n^{\alpha\beta\gamma\delta}\left(\delta\boldsymbol{\varphi}_{,\gamma}\cdot\boldsymbol{\varphi}_{,\delta}+\boldsymbol{\varphi}_{,\gamma}\cdot\delta\boldsymbol{\varphi}_{,\delta}\right)\boldsymbol{\varphi}_{,\beta}\\
&+ \bar{j}\boldsymbol{n}^{\alpha}\cdot\boldsymbol{\varphi}^{,\beta}\delta\boldsymbol{\varphi}_{,\beta}\\
&+ \frac{\bar{j}_0}{\lambda_h}\lambda_{\mu}^{\beta}\mathcal{H}_m^{\alpha\mu\gamma\delta}\left(\delta\boldsymbol{\varphi}_{,\gamma}\cdot\boldsymbol{t}_{,\delta}+\boldsymbol{\varphi}_{,\gamma}\cdot\delta\boldsymbol{t}_{,\delta}\right)\boldsymbol{\varphi}_{,\beta}\\
&+ \bar{j}\lambda_h\tilde{m}^{\alpha\mu}\left(\delta\boldsymbol{t}_{,\mu}\cdot\boldsymbol{\varphi}^{,\beta}-\frac{\lambda_{\mu}^{\zeta}}{\lambda_h}\boldsymbol{\varphi}^{,\beta}\cdot\delta\boldsymbol{\varphi}_{,\zeta}\right)\boldsymbol{\varphi}_{,\beta}
\end{aligned} \tag{26}$$

with $\tilde{m}^{\alpha\mu}=\tilde{\boldsymbol{m}}^{\alpha}\cdot\boldsymbol{\varphi}^{,\mu}$, $\lambda_{\mu}^{\beta}=\lambda_h\boldsymbol{t}_{,\mu}\cdot\boldsymbol{\varphi}^{,\beta}$. This expression can be used for implementation of $a_{nI2}^{s}(\boldsymbol{\varphi}_h,\delta\boldsymbol{\varphi})$ (21).

Finally, the continuity of displacement field is ensured weakly by 7 interface terms given by equation (15-17) and (20-23). These expressions can be used to write a weak form of the problem (see [4] for more details),

$$\begin{aligned}
a_d^e(\boldsymbol{\varphi}_h,\delta\boldsymbol{\varphi}) &= -\sum_e a_n^e(\boldsymbol{\varphi}_h,\delta\boldsymbol{\varphi})-\sum_e a_m^e(\boldsymbol{\varphi}_h,\delta\boldsymbol{\varphi})-\sum_s a_{nI1}^s(\boldsymbol{\varphi}_h,\delta\boldsymbol{\varphi})\\
&-\sum_s a_{mI1}^s(\boldsymbol{\varphi}_h,\delta\boldsymbol{\varphi})-\sum_s a_{nI2}^s(\boldsymbol{\varphi}_h,\delta\boldsymbol{\varphi})-\sum_s a_{mI2}^s(\boldsymbol{\varphi}_h,\delta\boldsymbol{\varphi})\\
&-\sum_s a_{nI3}^s(\boldsymbol{\varphi}_h,\delta\boldsymbol{\varphi})-\sum_s a_{mI3}^s(\boldsymbol{\varphi}_h,\delta\boldsymbol{\varphi})+\sum_s a_{sI3}^s(\boldsymbol{\varphi}_h,\delta\boldsymbol{\varphi})
\end{aligned}$$

with the traditional inertial, membrane and bending bulk components from the shell theory,

$$a_d^e(\boldsymbol{\varphi}_h,\delta\boldsymbol{\varphi}) = \int_{\mathcal{A}_e}\bar{\rho}\ddot{\boldsymbol{\varphi}}\cdot\delta\boldsymbol{\varphi}d\mathcal{A}\,, \tag{27}$$

$$a_n^e(\boldsymbol{\varphi}_h,\delta\boldsymbol{\varphi}) = \int_{\mathcal{A}_e}\bar{j}\boldsymbol{n}^{\alpha}\left(\boldsymbol{\varphi}_h\right)\cdot\delta\boldsymbol{\varphi}_{,\alpha}d\mathcal{A}\,, \tag{28}$$

$$a_m^e(\boldsymbol{\varphi}_h,\delta\boldsymbol{\varphi}) = \int_{\mathcal{A}_e}\bar{j}\tilde{\boldsymbol{m}}^{\alpha}\left(\boldsymbol{\varphi}_h\right)\cdot\delta\left(\lambda_h\boldsymbol{t}_{,\alpha}\right)d\mathcal{A} \tag{29}$$

3.2 Benchmarks

To prove the ability of the presented method to simulate continuum mechanic problems, 2 benchmarks coming from literature are performed. They are illustrated on figure 2 and the different parameters for the geometries and elasto-plastic materials are given in table 1. For these examples the stability parameters are $\beta_1=\beta_2=100\beta_3=10$.

The first example is a simply supported square plate dynamically loaded with a constant pressure $p_0=20.7$ [bars]. This benchmark was performed before by Swaddiwudhipong *et al.* [16] and Belytschko *et al.* [17] and they calculated the deflection at the center of the plate. This example is simulated again with the discontinuous Galerkin implementation with the explicit temporal integration scheme of Hulbert-Chung [18] without numerical dissipation. The obtained results are in agreement with previous studies (see figure 2 b)).

The second one focuses on a pinched hemisphere, depicted on figure 2 c), and discretized with a unstructured third order mesh. It is loaded on two opposite diameters (one in tension, the other in compression) in a quasi static way. This example was performed before by Simo *et al.* [12] and closed results are obtained with the presented method (see figure 2 d)).

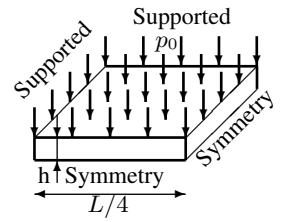

(a) Geometry of dynamic benchmark

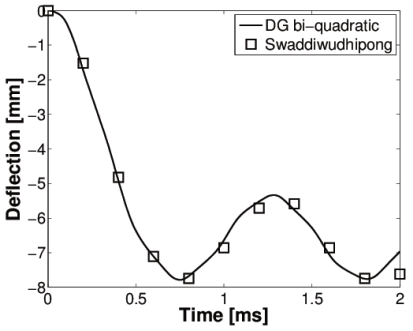

(b) Results of dynamic benchmark

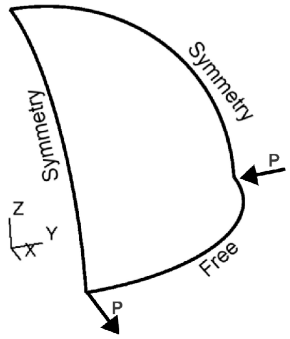

(c) Geometry of quasi-static benchmark

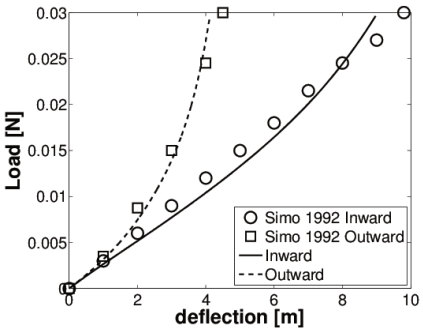

(d) Results of quasi-static benchmark

Figure 2: Discontinuous Galerkin framework shows good correlation with literature results

(a) Square plate

Geometry	
Length (L) [mm]	254
thickness (h) [mm]	12.7
Material	
density (ρ) [kg/m^3]	2768
Young modulus (E) [MPa]	69000
Poisson ratio (ν) [-]	0.3
Yield stress (σ_{y0}) [MPa]	207
Hardening modulus ($\overline{h}$) [MPa]	0

(b) Hemisphere

Geometry	
Radius (R) [m]	10
thickness (h) [m]	0.5
Material	
Young modulus (E) [Pa]	10
Poisson ratio (ν) [-]	0.2
Yield stress (σ_{y0}) [Pa]	0.2
Hardening modulus ($\overline{h}$) [Pa]	9

Table 1: Geometrical and material law parameters for continuum mechanic benchmarks

4 Application to fracture mechanic

The main advantage of a discontinuous Galerkin formulation is obviously its use for fracture mechanic applications. Indeed the presented framework can be coupled with an extrinsic cohesive law in a suitable way as no topological mesh modification is required to propagate a crack. In a recent paper [4] the authors presented a novel cohesive law dedicated to thin bodies formulation. The problem in the case of thin bodies is to propagate the crack through the implicitly modeled thickness. Indeed, the different behavior in traction and compression for crack propagation leads to the necessity to move the neutral axis during crack propagation. Moving this axis is not straightforward which motivated the development of a new cohesive law based on reduced stresses (6 - 8) which is energetically consistent (i.e. the model ensures the correct amount of energy released during crack propagation). This model is used to simulate the crack propagation in a cylinder after an inside blast. This example suggested by Larsson *et al.* [7] was previously used by the authors to validate their model of linear elastic shells [4]. The obtained results with elastic laws are not in correlation with experiments as mentioned by Larsson *et al.* who suggest to introduce elasto-plastic finite deformation model to study the cylinder in a more realistic way. The formulation developed herein is thus used to study this benchmark.

To avoid unphysical blow up of elements, an idea suggested by Zhou *et al.* [19] which uses a statistical distribution for fracture strength is considered. This one can vary in a range between its nominal value (here 10%) at each Gauss point of interface elements and is physically justified by the material imperfections which introduce such a distribution.

The cylinder has a diameter of 1.2 [m], is 1 [m] long and has a thickness of 1 [mm]. It exhibits an initial crack of 56 [mm] centered on its height. The material is the Al2024-T3 which has the following properties: Young modulus 73.1 [GPa], Poisson ratio 0.33 [-], density 2780 [kg/m^3], yield stress 350 [MPa], hardening modulus $800.$ [MPa], fracture strength[2] 650 [MPa] and fracture energy 19 [kJ/m^2]. Due to problem symmetry and to save computational time, only the top side of the cylinder is modeled with 2880 bi-cubic elements. The simulation is performed with the explicit Hulbert-Chung scheme [18] including a low numerical dissipation (spectral radius of 0.9). The blast is simulated thanks to the curve depicted on figure 3 a). The speed of crack propagation is studied on figure 3 b) which shows this relation for the experiment for the model of Larsson *et al.* [7] and for the presented DG/ECL framework with linear small strain and elasto-plastic finite deformation. As predict by Larsson *et al.* the introduction of plasticity allows to obtain results in agreement with experiment even if the speed at beginning of crack seems faster in our model. After a propagation of 0.18[m] the model matches quite well the experimental data.

5 Conclusion

This paper focuses on the extension to elasto-plasticity and finite deformations of a framework combining discontinuous Galerkin formulation of shells and extrinsic cohesive law. The obvious interest of the framework is its ability to simulate crack propagation. The recourse to discontinuous formulation allows to insert cohesive elements on the fly during the simulation without any modification of the mesh which is an issue with the continuous approach. As the elements are discontinuous it is mandatory to guarantee (weakly) the continuity to model correctly the continuum part of the deformation before the fracture. With regard to this end, the approach is extended here to elasto-plastic finite deformations and applied to numerical benchmarks coming from the literature.

The method, combining full discontinuous Galerkin formulation with extrinsic cohesive law, is able to match experiments as shown in the blasted cylinder example. Furthermore, the presented framework is suitable only for small scale yielding and other improvements are necessary to simulate crack propagation in ductile materials.

[2]The fracture strength is chosen following the work of Zavattieri [20] for aluminum 2024-T3

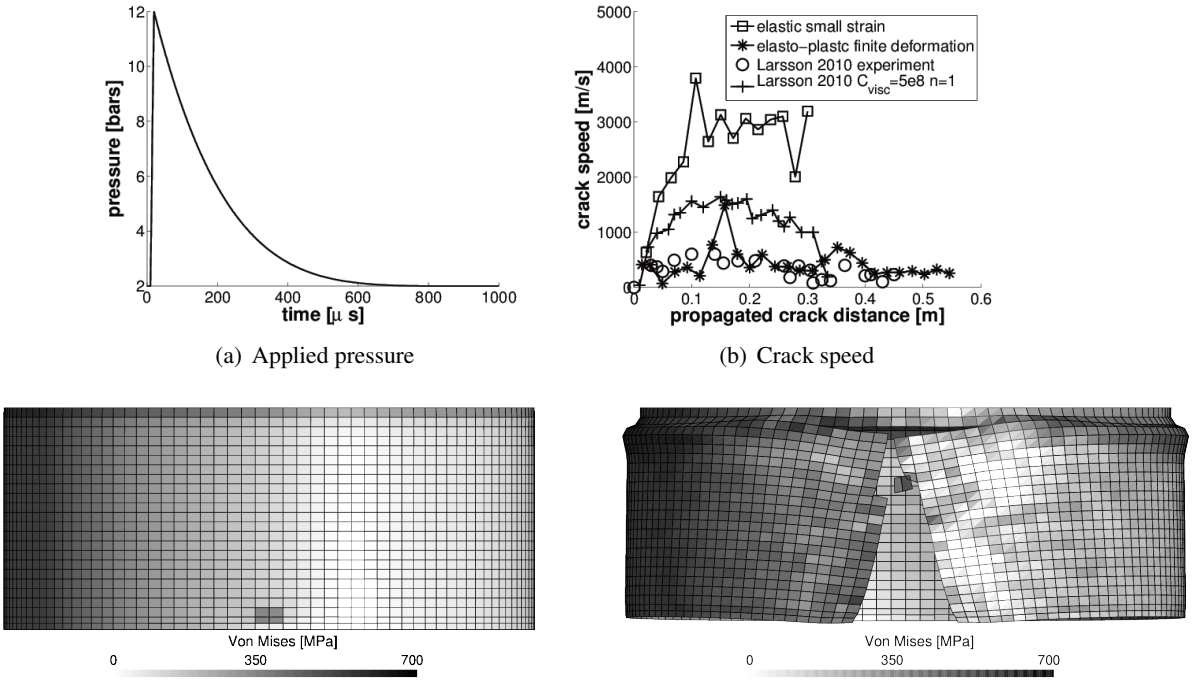

(a) Applied pressure

(b) Crack speed

(c) Cylinder at the beginning of simulation

(d) Cylinder at the end of simulation

Figure 3: Improvement of crack speed caption due to consideration of elasto-plastic finite deformations

References

[1] J. Mergheim, E. Kuhl, and P. Steinmann. A hybrid discontinuous galerkin/interface method for the computational modelling of failure. *Communications in Numerical Methods in Engineering*, 20(7):511–519, 2004.

[2] R. Radovitzky, A. Seagraves, A. Jerusalem, and L. Noels. A hybrid dg/cohesive method for modeling dynamic fracture of brittle solids. -, –.

[3] G. Becker and L. Noels. A fracture framework for euler-bernoulli beams based on a full discontinuous galerkin formulation/extrinsic cohesive law combination. *International Journal for Numerical Methods in Engineering*, 85(10):1227–1251, 2011.

[4] G. Becker, C. Geuzaine, and L. Noels. A one field full discontinuous galerkin method for kirchhoff-love shells applied to fracture mechanics. *Computer Methods in Applied Mechanics and Engineering*, In Press, Accepted Manuscript:–, 2011.

[5] G. Becker and L. Noels. A full discontinuous galerkin formulation of non-linear kirchhoff-love shells with elasto-plastic finite deformations. *In preparation*, 2011.

[6] L. Noels. A discontinuous galerkin formulation of non-linear kirchhoff-love shells. *International Journal for Numerical Methods in Engineering*, 78(3):296–323, 2009.

[7] Ragnar Larsson, Jesus Mediavilla, and Martin Fagerström. Dynamic fracture modeling in shell structures based on xfem. *Int. J. Numer. Meth. Engng.*, 86(4-5):499–527, 2011.

[8] J. C. Simo and D. D. Fox. On stress resultant geometrically exact shell model. part i: formulation and optimal parametrization. *Comput. Methods Appl. Mech. Eng.*, 72(3):267–304, 1989.

[9] J. C. Simo, D. D. Fox, and M. S. Rifai. On a stress resultant geometrically exact shell model. part ii: the linear theory; computational aspects. *Comput. Methods Appl. Mech. Eng.*, 73(1):53–92, 1989.

[10] J.C. Simo, D.D. Fox, and M.S. Rifai. On a stress resultant geometrically exact shell model. part iii: Computational aspects of the nonlinear theory. *Computer Methods in Applied Mechanics and Engineering*, 79(1):21 – 70, 1990.

[11] J. C. Simo, M. S. Rifai, and D. D. Fox. On a stress resultant geometrically exact shell model. part iv: Variable thickness shells with through-the-thickness stretching. *Computer Methods in Applied Mechanics and Engineering*, 81(1):91 – 126, 1990.

[12] J.C. Simo and J.G. Kennedy. On a stress resultant geometrically exact shell model. part v. nonlinear plasticity: formulation and integration algorithms. *Computer Methods in Applied Mechanics and Engineering*, 96(2):133 – 171, 1992.

[13] L. Noels and R. Radovitzky. A new discontinuous galerkin method for kirchhoff-love shells. *Computer Methods in Applied Mechanics and Engineering*, 197(33-40):2901–2929, 2008.

[14] Ralf Deiterding, Raul Radovitzky, Sean Mauch, Ludovic Noels, Julian Cummings, and Daniel Meiron. A virtual test facility for the efficient simulation of solid material response under strong shock and detonation wave loading. *Engineering with Computers*, 22(3):325–347–, 2006.

[15] A Cuitino and M Ortiz. A material-independent method for extending stress update algorithms from small-strain plasticity to finite plasticity with multiplicative kinematics. *Engineering Computations*, 9:437–451, 1992.

[16] S. Swaddiwudhipong and Z. S. Liu. Dynamic response of large strain elasto-plastic plate and shell structures. *Thin-Walled Structures*, 26(4):223 – 239, 1996.

[17] Ted Belytschko, Jerry I. Lin, and Tsay Chen-Shyh. Explicit algorithms for the nonlinear dynamics of shells. *Computer Methods in Applied Mechanics and Engineering*, 42(2):225 – 251, 1984.

[18] Gregory M. Hulbert and Jintai Chung. Explicit time integration algorithms for structural dynamics with optimal numerical dissipation. *Computer Methods in Applied Mechanics and Engineering*, 137(2):175 – 188, 1996.

[19] Fenghua Zhou and Jean-Francois Molinari. Stochastic fracture of ceramics under dynamic tensile loading. *International Journal of Solids and Structures*, 41(22-23):6573 – 6596, 2004.

[20] Pablo D. Zavattieri. Modeling of crack propagation in thin-walled structures using a cohesive model for shell elements. *J. Appl. Mech.*, 73(6):948–958, November 2006.